ELSEVIER

International Journal of Pharmaceutics 215 (2001) 251–262

international journal of pharmaceutics

www.elsevier.com/locate/ijpharm

Dehydration behavior of nedocromil magnesium pentahydrate

Haijian Zhu [a,*], David J.W. Grant [b]

[a] *Pharmaceutical Development Discovery Department, Glaxo Wellcome Inc., Five Moore Drive, Research Triangle Park, NC 27709, USA*

[b] *Department of Pharmaceutics, College of Pharmacy, University of Minnesota, 308 Harvard Street, SE., Minneapolis, MN 55455, USA*

Received 15 September 2000; received in revised form 7 December 2000; accepted 11 December 2000

Abstract

The dehydration of nedocromil magnesium (NM) pentahydrate proceeds in two steps, corresponding to the loss of four water molecules in the first step and one water molecule in the second step. The effects of temperature, particle size, sample weight, water vapor pressure and dehydration–rehydration cycle on both the kinetics and activation energy of the dehydration of NM pentahydrate were studied using isothermal TGA and temperature-ramp DSC analyzed by Kissinger's method. The dehydration kinetics for both steps are best described by the Avrami–Erofeev equations, suggesting a nucleation-controlled mechanism. The high activation energy for the second dehydration step indicates that the last water molecule, which is bonded both to a magnesium ion and to a carboxylate oxygen atom, is more 'tightly bound'. The activation energy decreased with increasing sample weight and decreasing particle size. The dehydration rate increased with decreasing water vapor pressure and with repetition of the dehydration–hydration cycle. Dynamic and isothermal PXRD, and ^{13}C solid-state NMR were employed to provide an insight into the dehydration mechanism and the nature of solid-state phase transformation during the dehydration. Molecular modeling with Cerius^2 was used to visualize the crystal structure and to construct the molecular packing diagram. A correlation was noted between the dehydration behavior and the bonding environment of the water molecules in the crystal structure.

Keywords: Dehydration; Hydration; Kinetics; Nedocromil magnesium pentahydrate

1. Introduction

The divalent nedocromil anion (9-ethyl-4,6-dioxo-10-propyl-4H, 6H-pyrano[3,2-g]quinoline-2,8-dicarboxylate, Scheme 1), has valuable pharmacological properties that lead to the dilation of airways (Cairn et al., 1985). The sodium salt is used in the treatment of reversible obstructive airways diseases such as asthma (Cairn et al., 1985). Since the nature of the salt form can influence the physicochemical and biological properties of a drug, selection of the optimum salt form

* Corresponding author. Tel.: +1-919-4837927; fax: +1-919-3151091.

E-mail address: hjz40534@glaxowellcome.com (H. Zhu).

0378-5173/01/$ - see front matter
PII: S0378-5173(00)00700-6

plays an essential role in drug development (Hirsch et al., 1978; Forbes et al., 1992). Nedocromil metal salts were found to crystallize from aqueous solution as hydrates (Zhu et al., 1996, 1997a,b). The physicochemical characterization of NM magnesium salt was presented in a previous paper (Zhu et al., 1996). Among the three NM hydrates described, the pentahydrate was found to be thermodynamically stable under ambient conditions. The dehydration of NM pentahydrate proceeds in two steps, corresponding to the loss of four water molecules in the first step and one water molecule in the second step (Zhu et al., 1996). An understanding of the critical factors involved in the dehydration of salt hydrates is essential for determining relative hydrate stability, and thus for optimizing salt selection.

The objective of this work is to examine the effects of temperature, particle size, sample weight, water vapor pressure and dehydration–rehydration cycling on both the kinetics and activation energy of dehydration of NM pentahydrate using isothermal TGA and temperature-ramp DSC analyzed by Kissinger's method (Kissinger, 1957). Dynamic and isothermal PXRD and ^{13}C solid-state NMR are employed to provide insight into the dehydration mechanisms and to probe any solid phase transformations during the dehydration processes. Molecular modeling with Cerius[2] was used to visualize the crystal structure and to construct the molecular packing diagram.

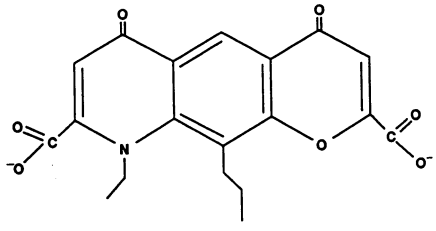

Scheme 1. Molecular structure of nedocromil anion

2. Materials and methods

2.1. Materials

NM pentahydrate was prepared as described in the previous paper (Zhu et al., 1996). The crystals were fractionated into three particle size ranges, 75–106 μm, 106–180 μm, and 180–250 μm, using USP standard sieves.

2.2. Thermal kinetic analysis

A DuPont 910 differential scanning calorimeter (TA Instruments, New Castle, DE) equipped with a data station (Thermal Analyst 2000, New Castle, DE) was used to record the DSC curves. The temperature axis and the cell constant of the DSC cell were calibrated with indium. Sample (3.0 ± 0.2 mg, 75–106 μm) in an open or crimped aluminum pan was heated at 2.5, 5, 10, 20 or 40°C/min under nitrogen purge 200 ml/min. The activation energy of each dehydration step was determined using Kissinger's method (Kissinger, 1957) in which the heating rate, ϕ, in °C/min, and the temperature at peak maximum, T_m, in degrees Kelvin, are plotted according to Eq. (1). This equation is derived with the assumption that the rate of reaction is maximal at the temperature at which the endothermic peak reaches a maximum. The activation energies were obtained from the slopes of the plots of $\ln(\phi/T_m^2)$ versus $1/T_m$. To examine the effects of particle size and sample weight on the activation energy, three particle sizes (75–106, 106–180, 180–250 μm) and three sample weights (3, 9, 20 mg) were used.

$$\mathrm{d}\ln(\phi/T_m^2)/\mathrm{d}(1/T_m) = -E_a/R. \quad (1)$$

2.3. Isothermal dehydration studies

A DuPont 951 thermogravimetric analyzer (TA instruments, New Castle, DE) linked to a Thermal Analyst 2000 data station was used to study the dehydration kinetics of NM pentahydrate. Samples (3.0 ± 0.2 mg, 75–106 μm) in open aluminum pans were heated under a dry nitrogen purge (200 ml/min). The weight loss, expressed as the fraction dehydrated, x, was plotted against

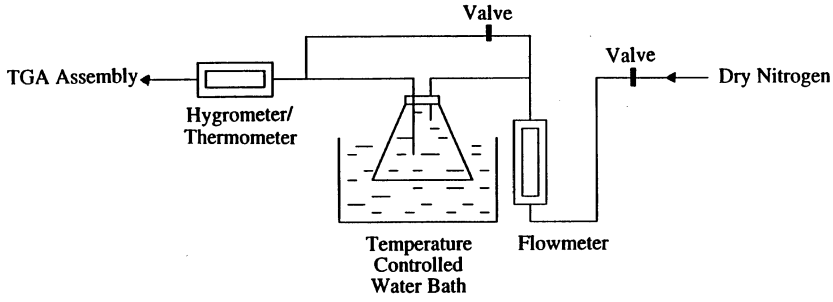

Scheme 2. Water vapor delivery system

time, t. For the first dehydration step, isothermal scans of x vs. t were obtained at fixed temperatures covering the range 59–97°C. The fraction dehydrated was calculated from the weight of water lost/maximum possible weight loss of water in dehydrating the pentahydrate to the monohydrate. Therefore, a 100% fraction dehydrated ($x = 1$) corresponds to the loss of four water molecules of hydration. For the second dehydration step, the samples were first heated to 90°C to allow completion of the first dehydration step. Analogous isothermal x versus t plots are obtained at fixed temperatures from 186 to 205°C. 100% fraction dehydrated ($x = 1$) corresponds to the loss of one water molecule of dehydration leading to NM anhydrate. Prior to each isothermal scan, the TGA furnace was rapidly heated at 150°C/min to the required study temperature and maintained at that temperature until each dehydration step was complete.

To examine the effects of particle size and sample weight on the dehydration kinetics, three particle sizes (75–106, 106–180, 180–250 μm) and three sample weights (3, 9, 20 mg) were used. To study the effect of water vapor pressure on the dehydration kinetics of NM pentahydrate, a water vapor delivery system (Scheme 2) was added to the TGA assembly to allow dynamic dehydration under controlled water vapor pressure. The desired water vapor pressure, p, was obtained by mixing dry nitrogen gas with nitrogen gas saturated with water vapor. The humidified nitrogen flowed at 200 ml/min through a hygrometer/thermometer (Fisher Scientific, WI) prior to entering the TGA balance. To examine the influence of dehydration–hydration cycling on the dehydration processes, the NM anhydrate produced after complete thermal dehydration was rehydrated at 98% RH at 22°C for 2 h before the second dehydration–hydration began. The rehydrated NM was crystallographically and stoichiometrically equivalent to the NM pentahydrate as confirmed by Karl–Fischer titrimetry and powder X-ray diffraction. For the first dehydration step, the samples were heated to 80°C and held isothermally. For the second dehydration step, the samples were first heated to 90°C to allow completion of the first dehydration step and then heated to 190°C and held isothermally.

2.4. Data analysis

The fraction dehydrated, x, was plotted as a function of time, t, according to the kinetic models of the reaction mechanisms known to occur in the solid state (Sharp et al., 1966; Byrn, 1982; Monkhouse and Van Campen, 1984). Three statistical parameters, standard deviation of regression, $S_{x/y}$, standard deviation of slope, S_b, and correlation coefficient, r, as well as plots of residuals against experimental values were determined to test the extent of conformity for the data to the kinetic models. The activation energies of dehydration were determined from Arrhenius plots of the rate constant derived from the statistically best-fitting mechanism.

2.5. Karl–Fischer titrimetry (KFT)

The amount of water in the NM hydrates were determined using a Moisture Meter (Mitsubishi CA-05, Mitsubishi Chemical Industries Ltd., Tokyo, Japan). Samples (2–6 mg) were accurately weighed and quickly transferred to the titration vessel containing anhydrous methanol prior to titration.

2.6. Powder X-ray diffraction (PXRD)

A diffractometer (Scintag 2000, Sunnyvale, CA) at 30 mA and 45 kV with CuKα radiation was used with a hot stage attachment to perform simultaneous X-ray diffraction dehydration studies. For non-isothermal studies in an open environment, samples were packed into a copper holder from which the water vapor could escape. For non-isothermal studies in a sealed environment, the sample was packed into a specially designed copper holder from which the water vapor could not escape. Each diffractogram was scanned from 5 to 15°, 2θ, at a rate of 5°/min with a counting time of 1 s. Each sample was heated to desired temperatures at a heating rate of 10°C/min to 80°C and held isothermally for 2 h, and was then heated at 10°C/min to 200°C and held isothermally for 1 h.

2.7. Polarized light microscopy

The NM crystals before or after dehydration were observed under an optical microscope (M3J, Wild Heerbrugg, Heerbrugg, Switzerland) equipped with a polarizer and an analyzer.

2.8. Hot stage microscopy (HSM)

The thermal events were observed on a hot stage (Mettler FP80, Mettler Instrument Corp., Highstwon, NJ) under a microscope (M3J, Wild Heerbrugg, Heerbrugg, Switzerland), with photoautomat and a camera. A single crystal of NM pentahydrate was immersed in high boiling silicone oil (Aldrich Chemical Co., Milwaukee, WI) and heated at a rate of 10°C/min. The liberation of bubbles corresponding to the escape of vapor from the solid enabled the dehydration events to be observed.

2.9. ^{13}C Solid-state nuclear magnetic resonance (NMR) spectroscopy

The NM pentahydrate was preheated to 100 or 240°C. The solid phases were then subjected to ^{13}C solid-state NMR. Each ^{13}C solid-state NMR spectrum was acquired at 75.7 MHz using a Chemagnetics CMX-300 spectrometer (Fort Collins, CO) and a Chemagnetics Pencil™ probe equipped with a 7.5 mm magic-angle spinning system with zirconia rotors. All spectra were acquired with cross-polarization, magic-angle spinning, and high-power ^{1}H decoupling. Spinning speeds were typically 5–6 kHz. Between 1024 and 2048 transitions were acquired with a repetition delay of 3 s, contact time of 5 ms, and pulse width of 4 μs. No apodization was applied to the free induction decay prior to the Fourier transform.

2.10. Molecular modeling

A commercial software package (Cerius^2, Molecular Simulations, Burlington, MA) was used to visualize the crystal structures and to draw molecular packing diagrams.

3. Results and discussion

3.1. Effect of temperature

Typical isothermal dehydration plots for the first and second dehydration steps are shown in Fig. 1a and b, respectively. In all cases, the shape of the curves is sigmoidal, and the dehydration rate increases with temperature. The curves are characterized by an induction period at low x values, a growth period with an inflection at intermediate values of x, and a decay period at high x values. The dehydration curves can be modeled by rate equations, which assure various reaction mechanisms known to occur in the solid state. For the first dehydration step, the dehydration kinetics are best described by the Avrami–Erofeev equation ($n=\frac{1}{2}$); the residuals are

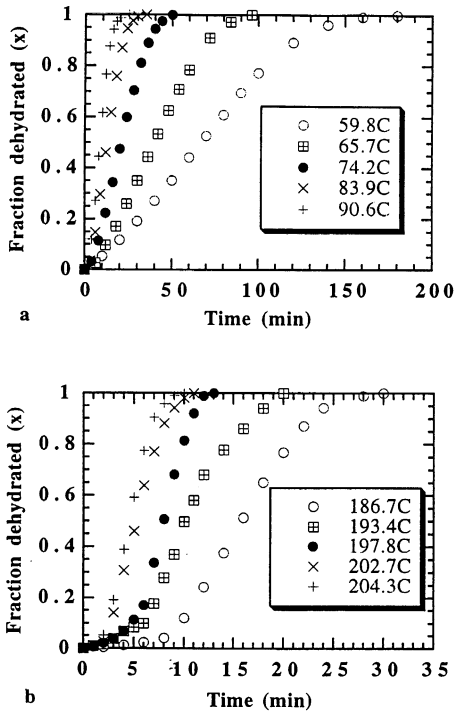

Fig. 1. Isothermal TGA curves for (a) the first and (b) the second dehydration steps of nedocromil magnesium pentahydrate.

randomly distributed, and no trend is seen. For the second dehydration step, the Prout–Tompkins and Avrami–Erofeev ($n = 1/3$) equations provide similar fits with a correlation coefficient, $r = 0.9930$. The residuals are randomly distributed, and no trends are seen for either model. However, smaller values of S_b and $S_{x/y}$ were obtained with the Avrami–Erofeev equation ($n = 1/3$). Thus, the Avrami–Erofeev equation ($n = 1/3$) was chosen preferentially for the dehydration kinetics of the second step. In studying the dehydration kinetics of theophylline monohydrate, Agbada and York (1994) suggested that great weighting should be given to S_b and $S_{x/y}$ as indications of goodness of fit. The Avarami–Erofeev equation assumes that the reaction is controlled by the growth and propagation of high-energy sites or nuclei (Garner, 1955; Mullin, 1993). This chain reaction is propagated from one molecule to the next until it is terminated when another product molecule is encountered (Wright, 1995). The dehydration mechanisms and statistical parameters obtained are summarized in Table 1.

Activation energies, E_a, obtained from Kissinger plots using crimped and open DSC pans, as well as those obtained from Arrhenius plots under isothermal TGA, are also tabulated in Table 1. In all cases, E_a for the second dehydration step is higher than that of the first step. The higher E_a for the second dehydration step indicates that the last water molecule, which is present as a monomer, i.e. and an isolated water molecule, is more tightly bound (Ojala et al., 1996). This conclusion agrees with the results of Whyte and Webster (1993), who, in a study of the bonding environment of the water molecules in nedocromil sodium trihydrate using the semi-empirical program MOPSC, showed that the energy required to stabilize the crystal lattice upon removal of water molecules in the tetramer is less than the energy required when the monomer is removed. Lumpkin and Perlmutter (1995) reported a similar case for barium chloride dihydrate, which showed a greater activation energy to remove the second water.

Table 1
Best-fitting mechanisms and statistical parameters for the dehydration of nedocromil magnesium pentahydrate

Dehydration step	Mechanism	r	$S_{x/y}$	S_b	E_a (kJ/mol) ($\pm$S.D., $n = 3$)		
					TGA (open pan)	DSC (crimped pan)	DSC (open pan)
NM.5H_2O $\rightarrow$ NM.H_2O	A2	0.9970	0.0050	0.0010	69.69 (2.34)	59.43 (1.32)	62.77 (1.34)
NM.H_2O $\rightarrow$ NM	A3	0.9930	0.0477	0.0077	120.64 (2.98)	101.69 (2.39)	111.56 (3.29)
	P1	0.9929	0.3175	0.0288			

The differences of activation energy determined from isothermal TGA, non-isothermal open-pan DSC and crimped-pan DSC studies may have mechanistic implications. In an open DSC pan, the dehydration of NM pentahydrate proceeds through an intermediate that undergoes an exothermic recrystallization process to the anhydrate. However, in a crimped pan, the water vapor cannot easily escape, so the recrystallization exotherm overlaps with the dehydration endotherm (Zhu et al., 1996). Under isothermal conditions, the dehydration and recrystallization processes may overlap, whereas under non-isothermal conditions, there is often a lag between them.

3.2. Effects of particle size and sample weight

Representative dehydration curves for NM pentahydrate of three sieve fractions (75–106, 106–180, 180–250 μm) and constant sample weight (3 mg) are shown in Fig. 2. As expected, the dehydration rate in both dehydration steps increases as the particle size decreases, primarily because of the increased surface area available for dehydration of the smaller particles. Representative dehydration curves for NM pentahydrate of three different sample weights (3, 9, and 20 mg) and particle size fraction 75–106 μm are shown in Fig. 3. The time required for each dehydration step is shorter for the 3 mg sample, implying a faster dehydration rate for the small sample weight.

The activation energies obtained from Kissinger plots using open pans with different sample weights and particle sized are shown in Table 2. The activation energies of dehydration decrease with decreasing particle size, as reported for the dehydration of sodium citrate dihydrate (Van Dooren, 1982). This could result from the enhanced dehydration due to the greater ratio of surface area/volume of the smaller particles.

The activation energies of dehydration decrease with increasing sample weight. This relationship between sample weight and activation energy of dehydration has also been observed by Agbada and York (1994) and has been attributed to the greater self-cooling effects of a larger sample mass in the endothermic reaction as well as to the varying sample geometry. The activation energy of dehydration, under given experimental conditions, will be affected by both particle size and sample weight. With a larger sample weight, the increased surface area associated with the smaller particles will promote dehydration and therefore reduce E_a. However, with a smaller sample weight, the accompanying reduction in self-cooling efficiency will tend to increase E_a. The balance between these two effects is determined by the experimental conditions and sample characteristics (Agbada and York, 1994).

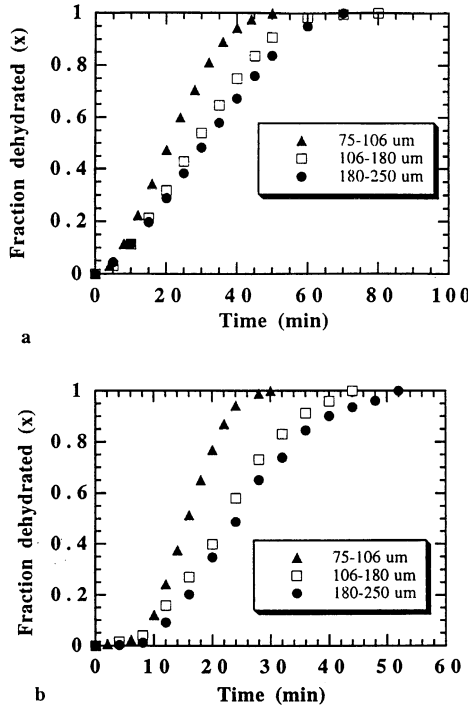

Fig. 2. Effect of particle size on dehydration kinetics of nedocromil magnesium pentahydrate (sample weight 3 mg): (a) first dehydration step (samples were heated to 80°C and held isothermally); (b) second dehydration step (each sample was heated to 90°C to allow completion of the first dehydration step and then heated to 190°C and held isothermally).

3.3. Effect of water vapor

The dehydration rate of NM pentahydrate was determined using isothermal TGA at 80°C under several constant water vapor pressures, which

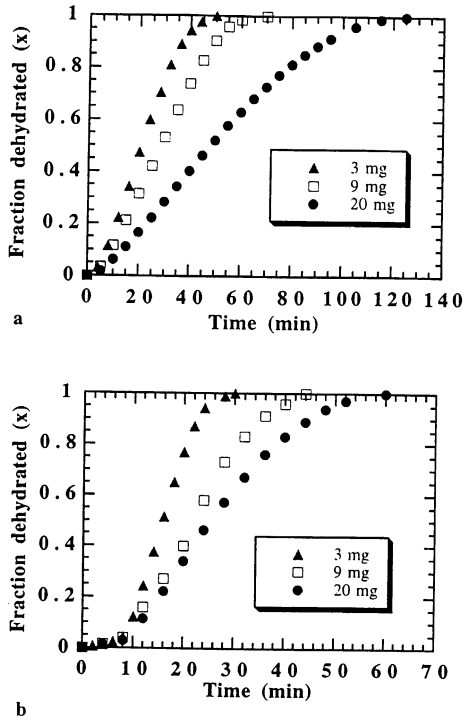

Fig. 3. Effect of sample weight on dehydration kinetics of nedocromil magnesium pentahydrate (particle size 75–106 μm): (a) first dehydration step (each sample was heated to 80°C and held isothermally); (b) second dehydration step (each sample was heated to 90°C to allow completion of the first dehydration step, then heated to 190°C and held isothermally).

range from 0 to 17.82 Torr. The kinetic data (Fig. 4) show a very pronounce dependency on the water vapor pressure. The dehydration rate monotonically decreases with increasing water vapor pressure, as expected for the reversible reaction. Moreover, the fraction dehydrated drops to very low level ($x = 0.3$) at the water vapor pressure of 17.82 Torr. The severe rate reduction is probably due to the water vapor pressure being at or near the pentahydrate–monohydrate equilibrium pressure so that the incomplete conversions correspond to equilibrium mixtures of the pentahydrate and the monohydrate. The non-monotonic rate pressure dependence (the Smith–Topley effects) (Topley and Smith, 1935) was not observed for the dehydration of NM pentahydrate over the range of water vapor pressures studied.

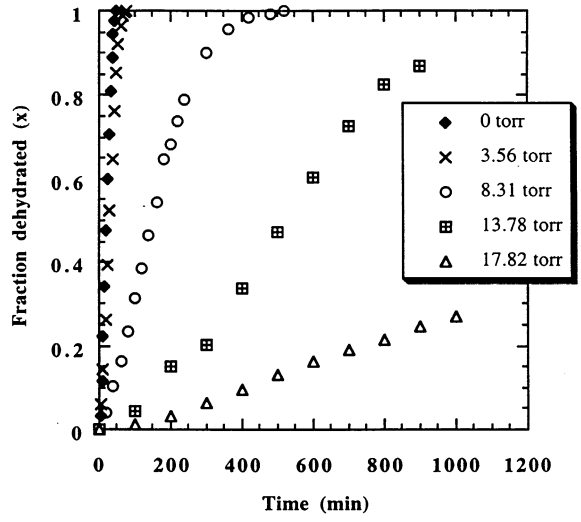

Fig. 4. Effect of water vapor pressure on dehydration kinetics of nedocromil magnesium pantahydrate at 80°C.

Table 2
Activation energies evaluated, by the Kissinger method in open pan DSC for different sample weights and particle sizes (by sieve fractions)

	Activation energy, E_a (kJ/mol) ($\pm$ S.D., $n = 3$)					
	3 mg		9 mg		20 mg	
	1st step	2nd step	1st step	2nd step	1st step	2nd step
75–106 μm	62.77 (1.34)	111.56 (3.29)	62.36 (0.78)	100.79 (3.47)	59.86 (2.12)	95.76 (3.56)
106–180 μm	64.46 (0.98)	114.96 (2.87)	62.56 (1.23)	103.34 (4.15)	61.65 (1.89)	96.30 (2.97)
180–250 μm	66.52 (2.12)	119.30 (4.19)	64.05 (1.98)	111.32 (2.89)	62.96 (2.18)	98.34 (4.17)

3.4. Effect of dehydration–hydration cycling

The effect of cycling on the dehydration reaction of NM pentahydrate is shown in Fig. 5. The first cycle exhibits a larger increase in the dehydration rate followed by a smaller increase in the second cycle. Cycling generates large cracks in the particle surface and significantly reduces the particle size, as confirmed by polarized light microscopy. In the second cycle, there must exist a much larger total surface area as compared to the original crystal in which the dehydration is initiated. The elimination of the induction period suggests that the intrinsic reactivity is subsequently enhanced. The relative increase in particle reaction rate is much less for the second cycles. It appears that most of the increase in intrinsic reactivity is realized during the first rehydration and second dehydration and that the total degree of enhancement after many cycles is effectively finite. The manner in which the intrinsic reactivity is increased by cycling or decreased by high-temperature heating is probably related to the defect structure and diffusional processes within the dehydrated material. Processes that produce lattice defects or enhance the diffusion rate increase the intrinsic reactivity, whereas those that destroy defects or increase diffusional resistance tend to decrease the intrinsic reactivity.

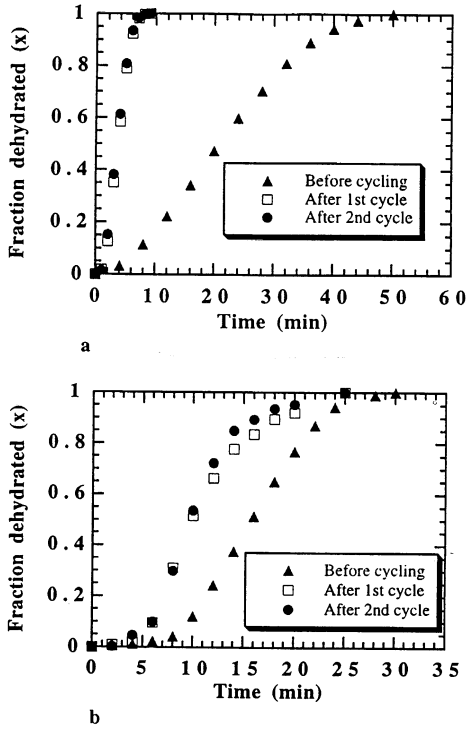

Fig. 5. Effect of dehydration–hydration cycling on dehydration kinetics of nedocromil magnesium pentahydrate: (a) first dehydration step (each sample was heated to 80°C and held isothermally); (b) second dehydration step (each sample was heated to 90°C to allow completion of the first dehydration step and then heated to 190°C and held isothermally).

3.5. Effects of structural changes

A simultaneous PXRD and thermal analysis of the NM pentahydrate dehydration was carried out under dry nitrogen purge, while the temperature was varied at a rate of 10°C/min from the ambient to 250°C. The PXRD peak from each solid was monitored as the dehydration progressed. The dehydration proceeded in a stepwise manner (Fig. 6a): the pentahydrate peak ($2\theta = 11.0°$) began to diminish and disappeared at 120°C, at which point, the monohydrate peak ($2\theta = 11.6°$) became evident; the monohydrate peak intensified until 224 and 240°C and further intensified to a greater value than before at 240°C. This effect appears to be due to the destruction of lattice defects by a recrystallizaiton process at high temperatures. It is postulated that the change in intensity of the anhydrate peak that occurs between 224 and 240°C is associated with arrangements of the anhydrous form. The recrystallization of NM anhydrate was observed in DSC with a small exotherm after the dehydration endotherm. The solid phases after heating NM pentahydrate to 100 and 240°C were characterized by ^{13}C solid-state NMR; the broadening and splitting of the various resonance of the solid phases are compared (Fig. 7), indicating changes of crystal structure during dehydration. The resemblance of the solid-state NMR spectra for the solid phases obtained by heating NM pentahydrate at 100°C (corresponding to NM monohydrate) and at 240°C (corresponding to NM anhydrate) suggests that NM monohydrate has a crystal structure similar to that of NM anhydrate, as indicated by variable-temperature PXRD (Fig. 6).

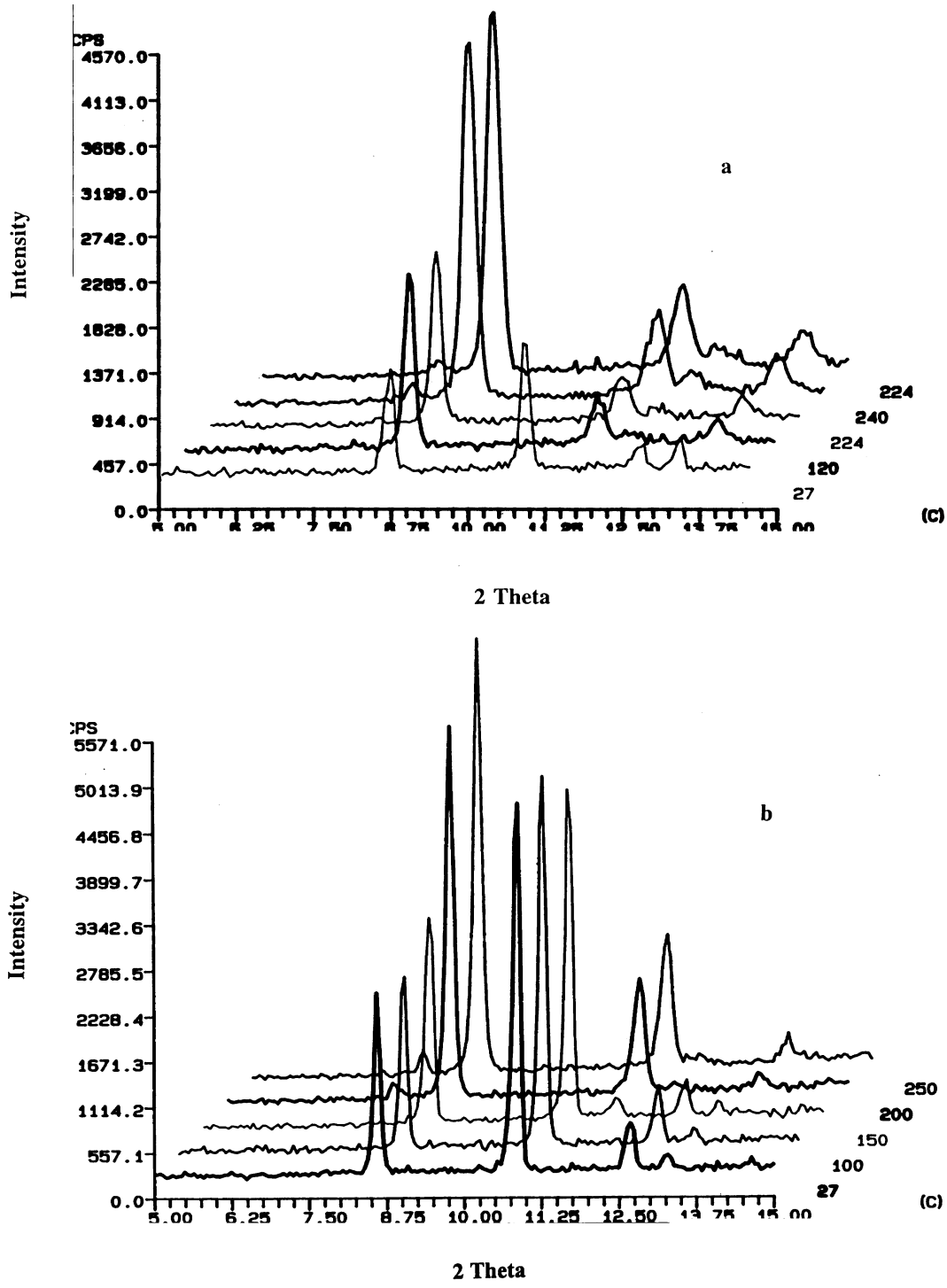

Fig. 6. Three-dimensional plots of diffracted intensity versus diffraction angle (2θ) and temperature (°C) showing: (a) the variable temperature under ambient atmosphere; (b) variable temperature in a closed system from which water vapor could not escape; (c) isothermal temperature under ambient atmosphere powder X-ray diffraction patterns of the nedocromil magnesium pentahydrate

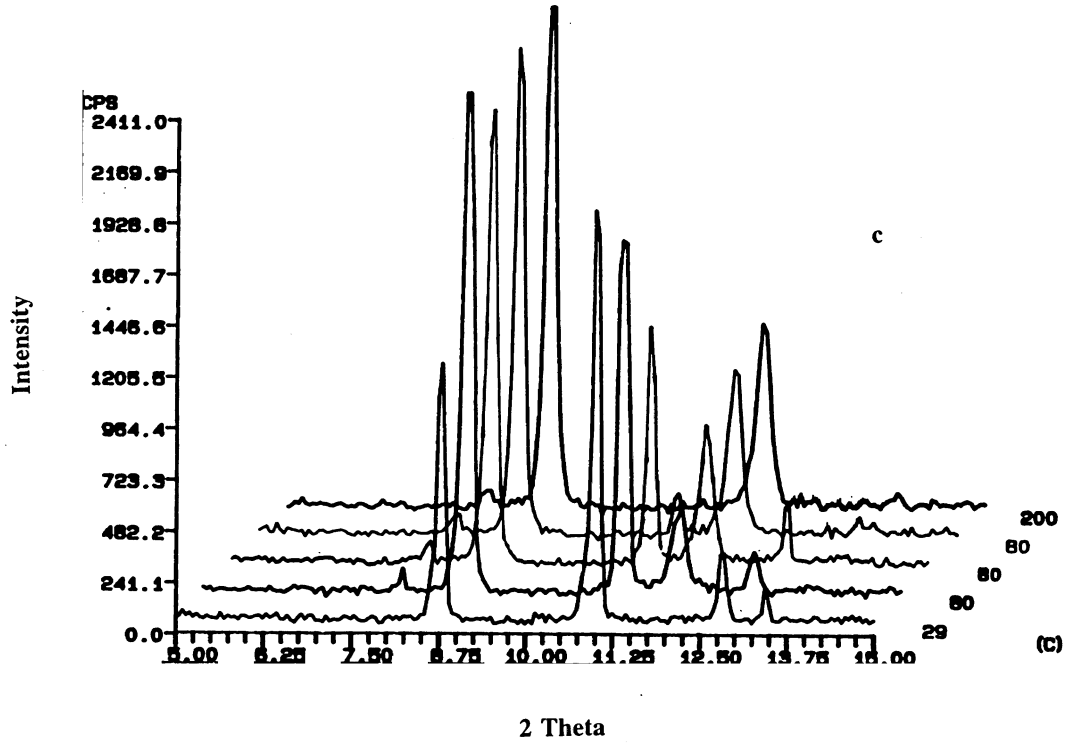

Fig. 6. (*Continued*)

The structural change during non-isothermal dehydration in a closed system was monitored after packing the sample in a specially fabricated X-ray holder covered with polyester film, from which water vapor could not escape. The dehydration was also found to proceed in a stepwise manner (Fig. 6b); the pentahydrate peak began to diminish, and the monohydrate peak became evident; the monohydrate peak intensified until 150°C. However, no increase in intensity of the anhydrate peak in PXRD occurred between 200 and 250°C, which is associated with the recrystallization of the anhydrate after the dehydration. In the presence of the generated water vapor pressure, the dehydration and recrystallization processes overlap.

The structural change during isothermal dehydration at 80°C was also monitored by simultaneous PXRD under dry nitrogen. The crystalline monohydrate PXRD pattern was observed at conversion and grew in intensity as the dehydration proceeded (Fig. 6c). When the crystalline monohydrate was heated to 200°C and held isothermally for 1 h, the anhydrate was obtained. No increase in intensity due to recrystallization was observed.

The pentahydrate before and after the dehydration–rehydration cycle were subjected to PXRD analysis. The pentahydrate after cycling showed broader peaks and lower intensities. The existence of amorphous material or a decrease of particle size may be attributed to the significantly decreased intensity in PXRD, as confirmed by polarized light microscopy.

3.6. Crystal structure and dehydration behavior

The crystal structure of NM pentahydrate was determined previously (Ojala et al., 1996). The intermolecular distances and bonding environments of water molecules in the NM pentahydrate were also reported in the paper. It was shown that

all five water molecules in NM are present in a different bonding environment. The water molecules O1W, O2W, O3W and O5W are connected to each other and form a tetrameric chain. The water molecule O4W links to the magnesium ion to the carboxyl oxygen and is the only water molecule that is not attached to any other water molecules and, hence, is present as a monomer in the crystal structure. Comparison of the thermal analysis results for NM with the bonding environment of its water molecules suggests that the water molecule comprising O4W may be the one that is tightly bound and released during the second dehydration step.

The changes in a single crystal of NM pentahydrate during the dehydration steps were observed under the hot stage microscope. At 94°C, the crystal became cloudy, corresponding to a phase transformation to the lower hydrate. The appearance of the bubbles actually began at 130°C, from both the needle axis (*a*-axis) and the side of the crystal (*b* or *c*-axis). For the pentahydrate crystal, the water molecules are arranged along the *a* and *b*-axes, probably because of the proximity of the hydrophobic ethyl and propyl side chains. Therefore, the water molecules probably travel along the *a* and *b*-axes. The highest rate of dehydration occurs at 157°C. The crystal further breaks into

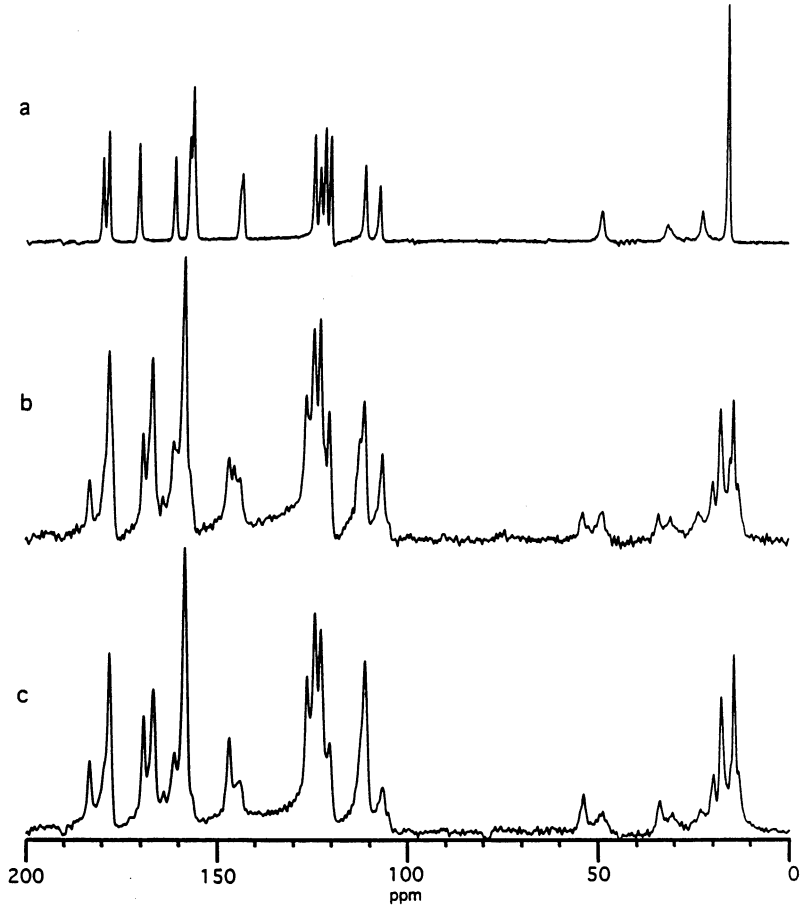

Fig. 7. ^{13}C solid-state NMR spectra of the nedocromil magnesium pentahydrates at different temperatures: (a) 23°C; (b) 100°C; (c) 240°C

many fragments until the last water is lost from the fragmented crystal structure at 273°C, indicating that the last mole of water in the pentahydrate is essential for the integrity of the crystal. On further heating to 290°C, these fragments darken due to the decomposition that follows the final dehydration.

4. Conclusions

NM pentahydrate exhibits two dehydration steps: the first step, $NM{\cdot}5H_2O \rightarrow NM{\cdot}H_2O + 4H_2O$; the second step, $NM{\cdot}H_2O \rightarrow NM + H_2O$. The higher activation energy for the second step indicates that the last water molecule is more tightly bound. The kinetics of both dehydration steps follow Avarami–Erofeev equations, suggesting nucleation-controlled mechanisms. The activation energies of dehydration decrease with decreasing particle size and increasing sample weight. The dehydration rate monotonically decreases with increasing water vapor pressure, as expected for the reversible reaction. The first cycle exhibits a larger increase in the dehydration rate followed by a smaller increase in the second cycle. NM monohydrate and anhydrate, both produced by thermal dehydration, have similar structures. Variable-temperature PXRD, ^{13}C sold-state NMR and HSM are complementary to thermal analysis for studying the dehydration mechanism and phase transformation of NM pentahydrate.

Acknowledgements

We thank Eric Munson and Brian Padden, Department of Chemistry, University of Minnesota, for collecting the ^{13}C solid-state NMR data. We also thank Fison, plc, for a gift of nedocromil sodium.

References

Agbada, O.C., York, P., 1994. Dehydration of theophylline monohydrate powder — effects of particle size and sample weight. Int. J. Pharm. 106, 33–40.

Byrn, S.R., 1982. Solid State Chemistry of Drugs. Academic Press, New York, pp. 59–74, 149–186.

Cairn, H., Cox, D., Gould, K.J., Ingall, A.H., Suschitzky, J.L., 1985. New antiallergic pyronol[3,2-g]quinoline-2,8-dicarboxylic acids with potential for the tropical treatment of asthma. J. Med. Chem. 28, 1832–1842.

Forbes, R.T, York, P., Fawcett, V., Shields, L., 1992. Physicochemical properties of salts of *p*-aminosalicylic acid. I. Correlation of crystal structure and hydrate stability. Pharm. Res. 9, 1428–1435.

Garner, W., 1955. Kinetics of endothermic solid reactions. In: Garner, W. (Ed.), Chemistry of the Solid State. Academic Press, New York, pp. 232–253.

Hirsch, C.A., Messenger, R.J., Brannon, J.L., 1978. Fenoprofen: Drug form selection and prefomulation stability studies. J. Pharm. Sci. 67, 231–236.

Kissinger, H., 1957. Reaction kinetics in differential thermal analysis. Anal. Chem. 29, 1702–1706.

Lumpkin, J.A., Perlmutter, D.D., 1995. Thermal and water vapor effects on the rate of the dehydration reactions of barium chloride. Thermochim. Acta 249, 335–349.

Monkhouse, D., Van Campen, L., 1984. Solid state reactions — theoretical and experimental aspects. Drug Dev. Ind. Pharm. 10, 1175–1276.

Mullin, J., 1993. Crystallization, third ed. Butterworth-Heinemann, Oxford, pp. 24–27, 104, 105.

Ojala, W.H., Khankari, R.K., Grant, D.J.W., Gleason, W.B., 1996. Crystal structures and physical chemical properties of nedocromil zinc heptahydrate and nedocromil magnesium pentahydrate. J. Chem. Cryst. 26, 167–178.

Sharp, J.H., Brindley, G.W., Achar, B.N.N., 1966. Numerical data for some commonly used solid state reaction equations. J. Am. Ceram. Soc. 49, 379–382.

Topley, B., Smith, M.L., 1935. Kinetics of salt-hydrate dissociation: MnC2O4.2H2O = MnC2O4 + 2H2O. J. Am. Chem. Soc. 57, 321–325.

Van Dooren, A.A., 1982. Effect of operational factors on kinetic parameters determined with DSC. In: Miller, B. (Ed.), Proc. 7th. Int. Conf. Thermal Analysis, vol. 1. Wiley, Chichester, UK, pp. 80–84.

Whyte, S., Webster, B., 1993. Scientific Project Thesis, Chemistry Department, University of Glasgow, UK.

Wright, J., 1995. Molecular Crystals, second ed. Cambridge University Press, Cambridge, pp. 50–70, 120–141.

Zhu, H., Khankari, R.K., Padden, B.E., Munson, E.J., Gleason, W.B., Grand, D.J.W., 1996. Physicochemical characterization of nedocromil bivalent metal salt hydrates: 1. nedocromil magnesium. J. Pharm. Sci. 85, 1026–1034.

Zhu, H, Padden, B.E., Munson, E.J., Grant, D.J.W., 1997a. Physicochemical characterization of nedocromil bivalent metal salt hydrates 2. nedocromil zinc. J. Pharm. Sci. 86, 418–429.

Zhu, H, Halfen, J.A., Young, V.G., Jr, Padden, B.E., Munson, E.J., Grant, D.J.W., 1997b. Physicochemical characterization of nedocromil bivalent metal salt hydrates 3. nedocromil calcium. J. Pharm. Sci. 86, 1439–1447.